



Published in final edited form as:

*Cell Mol Bioeng.* 2017 October ; 10(5): 451–462. doi:10.1007/s12195-017-0494-7.

## Immunomodulatory Effects of Human Cryopreserved Viable Amniotic Membrane in a Pro-Inflammatory Environment *In Vitro*

Claire E. Witherel<sup>1</sup>, Tony Yu<sup>1</sup>, Mark Concannon<sup>1</sup>, Will Dampier<sup>2</sup>, and Kara L. Spiller<sup>1</sup>

<sup>1</sup>School of Biomedical Engineering, Science and Health Systems, Drexel University, 3141 Chestnut Street, Philadelphia, PA 19104, USA

<sup>2</sup>Department of Microbiology and Immunology, Drexel University College of Medicine, Philadelphia, PA, USA

### Abstract

**Introduction**—Chronic wounds remain a major clinical challenge. Human cryopreserved viable amniotic membrane (hCVAM) is among the most successful therapies, but the mechanisms of action remain loosely defined. Because proper regulation of macrophage behavior is critical for wound healing with biomaterial therapies, we hypothesized that hCVAM would positively regulate macrophage behavior *in vitro*, and that soluble factors released from the hCVAM would be important for this effect.

**Materials and Methods**—Primary human pro-inflammatory (M1) macrophages were seeded directly onto intact hCVAM or cultured in separation *via* transwell inserts (Soluble Factors) in the presence of pro-inflammatory stimuli (interferon- $\gamma$  and lipopolysaccharide) to simulate the chronic wound environment. Macrophages were characterized after 1 and 6 days using multiplex gene expression analysis of 37 macrophage phenotype- and angiogenesis-related genes *via* NanoString™, and protein content from conditioned media collected at days 1, 3 and 6 was analyzed *via* enzyme linked immunosorbent assays.

**Results and Discussion**—Gene expression analysis showed that Soluble Factors promoted significant upregulation of pro-inflammatory marker *IL1B* on day 1 yet downregulation of *TNF* on day 6 compared to the M1 macrophage control. In contrast, intact hCVAM, which includes both extracellular matrix, viable cells, and soluble factors, promoted downregulation of pro-inflammatory markers *TNF*, *CCL5* and *CCR7* on day 1 and endothelial receptor *TIE1* on day 6,

---

Address correspondence to Kara L. Spiller, School of Biomedical Engineering, Science and Health Systems, Drexel University, 3141 Chestnut Street, Philadelphia, PA 19104, USA. [spiller@drexel.edu](mailto:spiller@drexel.edu).

#### ELECTRONIC SUPPLEMENTARY MATERIAL

The online version of this article (doi:10.1007/s12195-017-0494-7) contains supplementary material, which is available to authorized users.

#### CONFLICT OF INTEREST

KLS discloses a potential conflict of interest: this study was funded in large part by Osiris Therapeutics, Inc. The study was designed by KLS and CEW, with some input from Osiris with respect to the potential impact of different experiments. Employees from Osiris had no part in interpretation of the study's results. CEW, TY, MC, and WD declare that they have no conflicts of interest.

#### ETHICAL APPROVAL

Deidentified hCVAM samples were provided by Osiris Therapeutics as commercially available materials. De-identified human monocytes were purchased from the University of Pennsylvania Human Immunology Core. As such both human materials are exempt from review by the Institutional Review Board. No animal experiments were conducted for this article.

and upregulation of the anti-inflammatory marker *IL10* on day 6 compared to the M1 Control. Other genes related to inflammation and angiogenesis (*MMP9*, *VEGF*, *SPP1*, *TGFBI*, etc.) were differentially regulated between the Soluble Factors and intact hCVAM groups at both time points, though they were not expressed at significantly different levels compared to the M1 Control. Interestingly, Soluble Factors promoted increased secretion of the proinflammatory cytokine tumor necrosis factor- $\alpha$  (TNF- $\alpha$ ), while direct contact with hCVAM inhibited secretion of TNF, relative to the M1 Control. Both Soluble Factors and intact hCVAM inhibited secretion of MMP9 and VEGF, pro-inflammatory proteins that are critical for angiogenesis and remodeling, compared to the M1 Control, with intact hCVAM having a stronger effect.

**Conclusions**—In a simulated pro-inflammatory environment, intact hCVAM has distinct anti-inflammatory effects on primary human macrophages, and direct macrophage contact with intact hCVAM is required for these effects. These findings are important for the design of next generation immunomodulatory biomaterials for wound repair and regenerative medicine that may include living cells, soluble factors, or a controlled drug delivery system.

### Keywords

Macrophage; Cell–biomaterial interactions; Gene expression; Inflammation; Wound healing

## INTRODUCTION

Chronic wounds continue to be a major clinical problem affecting millions of patients and costing over \$10.5 billion every year in the US alone.<sup>30,43</sup> Human amniotic membrane (hAM), which is the innermost, avascular layer of the placenta, is composed of two main components: a matrix of extracellular matrix (ECM) proteins and a cellular layer consisting of epithelial cells, neonatal fibroblasts and mesenchymal stem cells (MSCs). hAM has been used as a treatment for chronic wounds for more than a century.<sup>11</sup> More recently it has regained traction as a chronic wound graft and dressing due to its ease of availability, advancements in tissue preservation, its efficacy in treating burns and ophthalmic disorders,<sup>38</sup> and association with a myriad of beneficial properties, including anti-inflammatory,<sup>16</sup> anti-scarring,<sup>49</sup> antibacterial,<sup>48</sup> and proangiogenic<sup>37</sup> behavior. Despite the appeal of hAM and positive clinical outcomes, there remains a limited understanding of its mechanisms of action in chronic wound healing.<sup>26</sup>

Currently, there are over 25 placental wound care products on the market<sup>14</sup>; one of the most successful is human cryopreserved, viable amniotic membrane (hCVAM), which retains cellular viability post-thaw while maintaining a shelf life comparable to other chronic wound treatments, and has shown efficacy compared to the standard of care in clinical trials.<sup>14,22,39</sup> The mechanisms behind the pro-healing effects of hCVAM are poorly understood, and may derive from soluble factors released either from the ECM or from the cells within the membrane, the ECM itself, or synergistic effects of all three sources. In a recent study, a novel comparative effectiveness research technique was used to perform a retrospective non-randomized investigation to compare clinical trial data from chronic wound patients treated with hCVAM or a dehydrated-hAM.<sup>8,20</sup> The results showed that wounds treated with hCVAM closed at a significantly higher rate (63%) than those treated with the dehydrated membrane (18.2%) over 12 weeks.<sup>20</sup> Additionally, *in vitro* studies showed that hCVAM

released lower levels of profibrotic transforming growth factor- $\beta$ 1 (TGFB1), as well as decreased levels of pro-inflammatory factors including interferon- $\gamma$  (IFNG), chemokine (C-C motif) ligand 5 (CCL5), epidermal growth factor (EGF), and thrombopoietin, compared to devitalized hAM.<sup>56</sup> On the other hand, hAM-derived ECM itself has been shown to promote enhanced cell proliferation compared to intact hCVAM.<sup>53</sup> While this study and others have shown positive effects of hAM-derived ECM or in combination with MCSs or other biomaterials,<sup>15,18,27,53,54</sup> the processes of decellularization, devitalization, or dehydration have been shown to significantly alter the ECM architecture and change the composition of hAM.<sup>10,17,21</sup> Thus, there remains a need to study the pro-healing effects of intact hCVAM in comparison to its released soluble factors.

The pro-healing effects of implanted or topically applied biomaterials are strongly associated with response of macrophages, the primary cell of the innate immune response,<sup>2,35</sup> which play a major role in wound healing, vascularization, and integration or failure of biomaterials.<sup>2,25,40</sup> Macrophages have been shown to exhibit different phenotypes *in vitro* and *in vivo* ranging from pro-inflammatory (M1) to anti-inflammatory (M2) as healing progresses.<sup>50,52,57</sup> While both M1 and M2 macrophages are present throughout the normal healing process, M1 macrophages primarily accumulate at early stages, around 1–5 days post injury, while M2 macrophages accumulate later, from 4 to 14 days *in vivo*.<sup>3</sup> Conversely, in chronic wounds, this transition in macrophage phenotype is dysregulated. Recent studies in mice and humans have shown that chronic wounds are stalled in a low-grade proinflammatory state, where M1 macrophages are found in significantly higher numbers relative to the M2 phenotype.<sup>13,31–34,36,44</sup> Additionally, two distinct subtypes of M2 phenotypes have been described, including M2a that are stimulated *in vitro* with interleukin-4 (IL4) and are associated with resolution of healing *in vivo*, and M2c, which are stimulated *in vitro* with IL10 and potentially involved in promoting angiogenesis and tissue remodeling at early stages of wound healing.<sup>28</sup> However, it is now widely accepted that macrophages frequently exist on a diverse spectrum of phenotypes with complex functions.<sup>35,46,58</sup>

Because of the critical role of macrophages in wound healing, we hypothesized that hCVAM would directly modulate macrophage behavior. In this study, we co-cultured primary human macrophages directly in contact with hCVAM or with soluble factors secreted from hCVAM *via* separation with transwell inserts to probe the potential mechanisms. It is important to note that direct contact with hCVAM also contains any soluble factors from the tissue or cells within, and that the effects of these signals may be synergistic. Macrophages were pre-polarized into the M1 phenotype using IFNG and lipopolysaccharide (LPS) prior to initiating the experiment to simulate a more clinically relevant scenario, as macrophages in chronic wounds have been identified to be primarily of the M1 phenotype.<sup>32,34,44</sup> The effects on macrophage behavior were analyzed over time using expression of a panel of 37 genes related to the M1, M2a, and M2c macrophage phenotypes (such as surface marker expression) and other aspects of inflammation and angiogenesis, as well as secretion of several key proteins. We chose to phenotype macrophages based primarily on gene expression, which has been proposed to be a more thorough method compared to analysis of surface markers<sup>46</sup> because macrophages often considerably change behavior without detectable changes in surface marker expression.<sup>45,47</sup>

## METHODS

### Cell Culture and Cell Seeding onto hCVAM

Primary human monocytes isolated peripheral blood from a single donor were purchased from University of Pennsylvania's Human Immunology Core and differentiated into unactivated M0 macrophages over 5 days and polarized into M1 macrophages for an additional 48 h (Fig. 1a), as previously described.<sup>47</sup> Briefly, monocytes were cultured in complete RPMI culture medium (cRPMI): RPMI 1640 with phenol red and L-glutamine supplemented with 10% heat-inactivated human serum, 1% penicillin streptomycin (Gibco™, Grand Island, NY), and 20 ng/mL of recombinant human macrophage colony stimulating factor (MCSF) (PeproTech®, Rocky Hill, NJ) for 5 days with a media change on the third day. On day 5, unactivated M0 macrophages were scraped, counted, and re-plated in cRPMI supplemented with 100 ng/mL of recombinant human IFNG (PeproTech®, Rocky Hill, NJ) and 100 ng/mL of LPS (Sigma Aldrich) (cRPMI-M1) for an additional two days to create M1 macrophages. After the full seven days, cells were scraped, counted, and used in subsequent experiments.

### Preparation of hCVAM and Experimental Group Organization

Samples of hCVAM (Grafix®, Osiris Therapeutics, Inc.) were generously donated by Osiris Therapeutics, Inc. (Columbia, MD), and stored at  $-80^{\circ}\text{C}$ . In preparation for *in vitro* culture, hCVAMs ( $n = 3$  donors) were thawed in their packaging in a  $37^{\circ}\text{C}$  water bath for approximately 1 min. Thawed packaged hCVAMs were quickly moved into a biological safety cabinet, removed from packaging and washed in sterile phosphate buffered saline (PBS) (cellgro®, Manassas, VA) in Petri dishes, which is consistent with clinical practice. The membranes were biopsy-punched using a 10 mm punch before being organized into experimental groups that were designed to isolate the effects of soluble factors released from the matrix and/or from cells within the matrix (Soluble Factors) in comparison to the effects of direct contact with intact hCVAM on macrophage behavior over time (Fig. 1b). For the intact hCVAM group ( $n = 3$  hCVAM donors;  $n = 3$  experimental replicates per donor per time point), M1 macrophages ( $5.0 \times 10^5$  cells in  $20 \mu\text{L}$  of cRPMI-M1) were seeded onto the stromal side of the membrane, which is the side placed onto chronic wounds clinically,<sup>22</sup> and allowed to attach to the membrane for 30–45 min in a  $37^{\circ}\text{C}$ , 5%  $\text{CO}_2$  cell culture incubator environment prior to the addition of 1 mL cRPMI-M1. For the Soluble Factors group ( $n = 3$  hCVAM donors,  $n = 3$  experimental replicates per donor per time point), M1 macrophages ( $5.0 \times 10^5$  cells) were plated in 1 mL of cRPMI-M1 in an ultra-low attachment tissue culture plate and allowed to sink to the bottom of the well before the adding a Millicell® cell culture insert (EMD Millipore Corporation, Billerica, MA) containing an hCVAM sample and 0.4 mL of cRPMI-M1. hCVAM controls and M1 Controls were also included. For the M1 Control group ( $n = 3$  experimental replicates per time point),  $5.0 \times 10^5$  M1 macrophages were plated in 1 mL of cRPMI-M1 in an ultra-low attachment tissue culture plate. For the hCVAM Control group ( $n = 3$  donors,  $n = 3$  experimental replicates per donor per time point), hCVAM was cultured in cRPMI-M1. All samples inclusive of any unadhered macrophages were collected for RNA extraction (hCVAM together with seeded macrophages and hCVAM alone in 1 mL of TRIzol Reagent (Life Technologies, Carlsbad, CA), or macrophages alone in  $350 \mu\text{L}$  of lysis buffer) on days 1 and 6 in Eppendorf tubes

and stored at  $-80^{\circ}\text{C}$ , while conditioned media was collected on days 1, 3, and 6 and frozen at  $-80^{\circ}\text{C}$  until further analysis (Fig. 1c).

### RNA Extraction and Multiplex Gene Expression Analysis

First, all samples were thawed on ice and homogenized in TRIzol<sup>®</sup> Reagent (Life Technologies, Carlsbad, CA). Sample homogenization for membrane-containing samples was performed using a Mini BeadBeater-16 (BioSpec Products, Bartlesville, OK) with three 2.3 mm stainless steel beads in each tube for 5–8 cycles of 10 s, placing samples on ice to maintain low temperature in between cycles. Next, 0.2 mL of chloroform was added to each sample and shaken rigorously by hand for 15 s, which were then incubated for 2–3 min at room temperature, and centrifuged for 15 min at  $4^{\circ}\text{C}$  with a speed of  $12,000\times g$ . The aqueous layer was then removed into a fresh tube. Cell-only samples were lysed by repeatedly pipetting in lysis buffer up and down, as opposed to homogenization with the bead beater. Equal parts 70% ethanol was added to all samples to obtain a final concentration of 35% ethanol, which was then loaded onto the RNeasy Mini spin columns (Qiagen<sup>®</sup>, Hilden, Germany), where RNA was purified according to the manufacturers' instructions. RNA from all samples was eluted in one volume of  $30\ \mu\text{L}$  and immediately frozen at  $-80^{\circ}\text{C}$  for future analysis. RNA was later thawed on ice and quantified using a NanoDrop 1000 (Thermo Scientific, Wilmington, DE) or a Bioanalyzer 2100 with RNA Nano 6000 kit (Agilent Technologies, Santa Clara, CA). Samples with 260/280 ratios between 1.7 and 2.2 or RIN numbers over 9.0 were considered pure and were utilized for multiplex gene expression analysis using NanoString (NanoString Technologies, Seattle, WA). Importantly, all hCVAM Control samples had extremely low concentrations of RNA ( $<4\ \text{ng/mL}$ ) confirmed with both Bioanalyzer and NanoDrop 1000; on the Bioanalyzer, samples had little to no visible bands in the RNA Nano chip above water-only controls. Therefore, hCVAM Controls were not included in the NanoString gene expression analysis, and gene expression data obtained from macrophage-seeded hCVAM samples are considered to derive primarily from the macrophages. NanoString gene expression analysis was performed according to the manufacturers' instructions, where 100 ng of RNA per sample was hybridized with the capture and reporter probes of the custom codeset (Table 1), inclusive of 37 endogenous genes, 5 housekeeping genes, 8 External RNA Control Consortium (ERCC) negative controls, and 6 ERCC positive controls. Samples from the M1 Control, Direct Contact, and Soluble Factors treatment groups were divided between 9 different NanoString cartridges, which only held 12 samples each, so that 1–6 samples from each treatment and/or donor within a time point were included in each cartridge. Raw count data was extracted from nSolver<sup>™</sup> Analysis Software 3.0 followed by quality control, normalization, and filtering, as described below.

### Data Normalization and Analysis

Raw count data from NanoString was first normalized to the ERCC positive controls per Nano-String's recommendation. First, the geometric mean of all positive controls for all samples was calculated and then divided by the geometric mean of each individual samples' ERCC positive controls, generating a ERCC positive control factor. All endogenous, housekeeping, ERCC negative and positive controls were multiplied by each samples' ERCC positive control factor to account for NanoString individual lane assay efficiency.

Positive control-normalized data was input into R Studio, where batch effects were removed for different lots of codeset and per NanoString cartridge, using the function *removeBatchEffect* within the *limma* package in R. The function to remove batch effects set the primary and secondary batch effects to two independent vectors and utilized a linear model to fit and correct the data. Next, data were normalized using the *voomWithQualityWeights* function within the *limma* package, which sets a weight factor to each sample treatment before performing a global normalization.<sup>24</sup> Next, the maximum value from all of the ERCC negative controls from each lane was subtracted from each sample to determine which genes were not expressed above the negative controls. If any biological replicate ( $n = 3$  donors of hCVAM) was missing two or more experimental replicates (of  $n = 3$  replicates per donor), then that biological replicate was excluded, and if more than 50% of all replicates were missing per gene, then the gene was excluded, which included *ALPL*, *ANGPT1*, *BGLAP*, *COL1A1*, *COL4A1*, *CTGF*, and *TEK*. Next, fold change values were calculated for each individual replicate compared to the averaged M1 Control for each gene and used to generate a heatmap using the *heatmap.2* function in R and a grouped column graph at each time point in GraphPad Prism 6. A dotted line at a fold change of 1.0 (or 0 on graphs of  $\text{Log}_2$ -transformed data of values normalized to the M1 Control) on each individual gene represents no change vs. the M1 Control. Principal component analysis was performed on the  $\text{Log}_2$  voom-normalized data as implemented in the *scikitlearn Decomposition* package with missing values imputed using nearest neighbor estimation as implemented in the *scikitlearn Preprocessing* package,<sup>1</sup> to holistically examine effects of treatment, donor, and time.

### Protein Secretion

Protein secretion from conditioned media from each treatment group was analyzed using enzyme-linked immunosorbent assay (ELISA) according to the manufacturers' instructions for human interleukin-10 (IL10), tumor necrosis factor- $\alpha$  (TNF- $\alpha$ ), and vascular endothelial growth factor (VEGF; PeproTech®, Rocky Hill, NJ) and matrix metalloproteinase-9 (MMP9; R&D Systems, Inc., Minneapolis, MN).

### Statistical Analysis

Normalized gene expression and protein secretion data were processed in GraphPad Prism 6.0. Statistical analysis of fold change data for individual gene expression was performed using a non-matched two-way analysis of variance (ANOVA) and Tukey's *post hoc* multiple comparisons test with an adjusted  $p$  value of 0.01 to determine significant differences between treatment groups within a time point. Analysis of protein secretion was performed using a non-matched two-way ANOVA and a Tukey's *post hoc* multiple comparisons test with an adjusted  $p$ -value of 0.01 to determine differences between treatment groups within a time point and over time. Statistical analysis of changes within a treatment group over time were performed utilizing a mixed effects model. Treatment and time were set as joint fixed effects while donor level variability was treated as a random effect. Regression was performed using the *statsmodels MixedML* package.<sup>42</sup>



## RESULTS

### Multiplex Gene Expression Analysis

No RNA was detected in the hCVAM-only control group *via* Bioanalyzer 2100 and NanoDrop 1000; therefore, all detected gene expression is considered to derive solely from macrophages. Normalized Nano-String gene expression data were first visualized using principal component analysis, which illustrated that there was no effect of hCVAM donor on global gene expression patterns (Fig. S1). A heatmap of all replicates organized by gene function revealed that the majority of genes were upregulated in the Soluble Factors group and downregulated in hCVAM group on day 1 compared to the M1 Control, while there appeared to be more subtle shifts in gene expression between treatment groups on day 6 (Fig. 2a). Plotting each gene individually at each time point (Figs. 2b and 2c) further confirmed these trends, and also showcased several genes with the most substantial changes. The genes with the most substantial differences between how direct contact with the hCVAM and Soluble Factors regulated macrophage behavior included *CCL5*, *VEGF*, *CCL22*, *MRC1*, *PDGFB*, *MMP9*, *VCAN*, *ANGPT2*, *BMP2*, *NOTCH1*, *PECAM1*, *RUNX2*, *SMAD1*, and *TGFB1* on day 1 and *CCL5*, *CD80*, *CD163*, *MMP7*, *PECAM1*, *SPP1*, and *VDR* on day 6 (Figs. 2b and 2c).

To explore individual gene expression differences, each gene was plotted over time and statistical analysis was conducted using a two-way ANOVA to assess differences between treatment groups within a time point, which identified 13 genes with significant differences (Fig. 3) and 17 genes without (Fig. S2); a mixed effects model was used to determine differences in expression over time (Fig. S3). Compared to the M1 Control, Soluble Factors promoted significant upregulation of the pro-inflammatory marker *IL1B* expression on day 1 ( $p < 0.01$ , indicated by # in Fig. 3a) but significant downregulation of the pro-inflammatory marker *TNF* expression on day 6 (Fig. 3b), while intact hCVAM promoted downregulation of pro-inflammatory markers *TNF*, *CCL5* and *CCR7* on day 1 (Figs. 3b–3d). Intact hCVAM also promoted upregulation of the anti-inflammatory marker *IL10* (Fig. 3e) and downregulation of the gene encoding tyrosine kinase receptor *TIE1* (Fig. 3f) compared to the M1 Control on day 6.

There were additional differences observed solely between the hCVAM and Soluble Factors groups at both time points, though these differences were not always significant compared to the M1 Control. Expression of *IL1B*, *TNF*, *CCL5*, *CCR7*, *IL10* (Figs. 3a–3e), *MMP9*, *VEGF*, *NOTCH1*, *RUNX2*, *SPP1*, and *TGFB1* (Figs. 3g–3l) was higher by macrophages in the Soluble Factors group on day 1 compared to the hCVAM group. At the day 6 time point, *CCL5* and *TIE1* were also expressed at higher levels in the Soluble Factors group relative to the hCVAM group (Figs. 3c and 3f). Only *IL10* and *CD80* were expressed at lower levels in the Soluble Factors group relative to the hCVAM group, and these changes were observed at day 6 (Figs. 3e and 3m). Changes in gene expression were also explored over time within a given treatment group (Fig. S3); interestingly, the only gene that changed significantly over time was *IL1B* in the Soluble Factors group (Fig. 3a).

### Protein Secretion Analysis

We next examined protein secretion of four proteins that are particularly important in inflammation, wound healing, and angiogenesis: TNF, IL10, MMP9 and VEGF (Fig. 4). Expression of these proteins on the gene level is shown in Figs. 3b, 3e, 3g, and 3h. Macrophages in the hCVAM group secreted significantly lower levels of TNF, VEGF, and MMP9 compared to the M1 Control and the Soluble Factors groups at all time points (Fig. 4). Additionally, macrophages in the Direct Contact group secreted significantly greater levels of IL10 compared to the Soluble Factors group at day 6 (Fig. 4b). Compared to the M1 Control at corresponding time points, macrophages in the Soluble Factors group secreted higher levels of TNF (all time points) and IL10 (day 3 only) and lower levels of MMP9 (day 1 only) and VEGF (day 3 only).

### DISCUSSION

In this study, we explored the immunomodulatory actions of soluble factors derived from hCVAM in comparison to intact hCVAM on the response of M1 macrophages, which dominate the chronic wound environment *in vivo*.<sup>32,44</sup> Direct contact with intact hCVAM, which includes both ECM- and soluble factor-derived signals, promoted more changes in gene expression and protein secretion than Soluble Factors. These changes resulted in a shift toward an anti-inflammatory phenotype, even in the continued presence of pro-inflammatory stimuli. Collectively, these results suggest that the immunomodulatory effects of hCVAM require direct contact with the membrane, which have important implications for the design of next generation bioactive, immunomodulatory chronic wound treatments.

Macrophages are highly influenced by their microenvironment, which includes their interaction with structures, cytokines, signals, cells, or foreign materials.<sup>23</sup> In keeping with the results shown in this study, recent studies have shown that ECM-derived signals are key modulators of macrophage behavior *in vitro* and *in vivo*. In one study, an acellular porcine bladder xenograft and rat body wall autograft promoted a more M2-like macrophage phenotype response (as measured *via* immunohistochemical staining with *CD163*) and were subsequently associated with a constructive remodeling healing outcomes in a rat abdominal wall repair model relative to their cellular counterparts.<sup>5,9</sup> In addition, macrophages co-cultured with four commercially available ECM-derived wound matrices *in vitro* exhibited hybrid macrophage phenotypes that correlated with the products' outcomes *in vivo*.<sup>55,58</sup> Collectively, these results illustrate the critical role of ECM-based biomaterials in modulating macrophage behavior for tissue repair.

The anti-inflammatory effects of hCVAM on macrophages that we report in this study are consistent with recent reports that have explored responses of other immune cells to hCVAM. For example, in one study peripheral blood mononuclear cells (PBMCs) were pretreated with LPS, activating the cells to secrete pro-inflammatory cytokines,<sup>19</sup> and co-cultured with either hCVAM or devitalized hAM pre-treated with TNF. hCVAM pre-treated with TNF promoted significantly higher levels of secretion of the anti-inflammatory factor IL10 compared to devitalized hAM pre-treated with TNF.<sup>11</sup> In another study, macrophages shifted to an anti-inflammatory phenotype when cultured in media conditioned by hAM-derived MSCs, even in the presence of pro-inflammatory stimuli.<sup>29</sup> In a study of diabetic



wound healing *in vivo*, authors micronized hCVAM *via* homogenization and filtration to obtain 300–600  $\mu\text{m}$  particles, which were compared to particles derived from devitalized AM in a murine full-thickness diabetic wound model.<sup>59</sup> The living micronized AM (LMAM), which retained cell viability, promoted significantly enhanced wound closure, increased recruitment of macrophages (F4/80<sup>+</sup>) that were predominately of an M2 phenotype (MRC1<sup>+</sup>), and reduced secretion of pro-inflammatory proteins [IL1B, interleukin-6 (IL6) and TNF] *in vivo* compared to amniotic membrane that was devitalized *via* multiple freeze/thaw cycles.<sup>59</sup> Furthermore, conditioned media from LMAM caused macrophages to significantly downregulate expression of the M1 marker *CCR7*, upregulate expression of the M2a marker *MRC1*, and increase secretion of factors involved in chemotaxis, inflammation and angiogenesis, relative to devitalized hAM.<sup>59</sup> Collectively, these studies and our results suggest that cell-hCVAM interactions promote an anti-inflammatory macrophage phenotype, even in the presence of pro-inflammatory stimuli.

The distinct changes in macrophage behavior, as measured by multiplex gene expression analysis and protein secretion, provide insight into the mechanisms of hAM-promoted chronic wound healing. Previous studies have shown that persistent, elevated TNF or blocked TNF have both been shown to be detrimental to angiogenesis and healing,<sup>6,51</sup> while an early, yet transient, release of TNF, has been shown to enhance healing.<sup>4,41</sup> These studies in combination with our work suggest that contact with hCVAM may play a unique role in modulating macrophage behavior *via* inhibition of TNF, which may minimize prolonged inflammation.<sup>41</sup> Significant early downregulation of pro-inflammatory cytokines and markers TNF, CCL5, and CCR7 suggests that intact hCVAM may drive macrophages away from an M1 macrophage phenotype.<sup>47</sup> While these effects may be beneficial for chronic wounds that are characterized by elevated inflammation, they may also have negative implications with respect to how macrophages handle bacterial infection.<sup>7</sup>

Lastly, there were limitations to this work. We attempted to simulate the chronic wound environment by conducting the experiments in the presence of the proinflammatory, M1-promoting stimuli IFNG and LPS, but even more anti-inflammatory effects might be observed in the absence of these signals. It would be interesting in future studies to investigate how macrophages of different phenotypes, including unactivated macrophages, differentially respond to hCVAM. Another limitation is that only a small number of genes and proteins was evaluated. Future work will explore a larger panel of genes related to inflammation and angiogenesis and include the use of functional assays, such as angiogenesis assays. Finally, there is always the possibility that *in vitro* results fail to accurately recapitulate interactions *in vivo*, where the microenvironment is considerably more complex. These limitations notwithstanding, this study illustrates that direct contact with hCVAM and soluble factors from hCVAM each have distinct roles in modulating macrophage behavior *in vitro*, with direct contact having more dominant effects in the continued presence of pro-inflammatory stimuli. These important, yet preliminary, findings lay the groundwork for more robust mechanistic studies of the immunomodulatory effects of hCVAM *in vivo*.

## Supplementary Material

Refer to Web version on PubMed Central for supplementary material.

## Acknowledgments

The authors would like to thank Yi Arnold-Duan and Matthew Moorman (Osiris Therapeutics, Inc.) for their helpful discussions and technical advice in handling hCVAM. This work was sponsored in part by Osiris Therapeutics, Inc., and by NHLBI Grant Number R01 HL130037 to KLS. CEW is grateful for the US Department of Education Graduate Assistance in Areas of National Need (GAANN) Interdisciplinary Collaboration and Research Enterprise (iCARE) Fellowship.

## ABBREVIATIONS

<b>hAM</b>	Human amniotic membrane
<b>ANOVA</b>	Analysis of variance
<b>CCL5</b>	Chemokine (C–C motif) ligand 5
<b>cRPMI</b>	Complete RPMI culture medium
<b>cRPMI-M1</b>	Complete RPMI culture medium supplemented with M1-stimulating cytokines
<b>ECM</b>	Extracellular matrix
<b>EGF</b>	Epidermal growth factor
<b>ELISA</b>	Enzyme-linked immunosorbent assay
<b>ERCC</b>	External RNA Control Consortium
<b>hCVAM</b>	Human cryopreserved amniotic membrane
<b>IFNG</b>	Interferon- $\gamma$
<b>IL4</b>	Interleukin-4
<b>IL8</b>	Interleukin-8
<b>IL10</b>	Interleukin-10
<b>IL1A</b>	Interleukin-1 $\alpha$
<b>IL1B</b>	Interleukin-1 $\beta$
<b>LPS</b>	Lipopolysaccharide
<b>LMAM</b>	Living micronized amniotic membrane
<b>MCSF</b>	Macrophage colony stimulating factor
<b>MMP9</b>	Matrix metalloproteinase-9
<b>MSCs</b>	Mesenchymal stem cells

<b>PBMCs</b>	Peripheral blood mononuclear cells
<b>PBS</b>	Phosphate buffered saline
<b>PDGFB</b>	Platelet derived growth factor
<b>PGE2</b>	Prostaglandin E2
<b>SEM</b>	Standard error of mean
<b>TGFB1</b>	Transforming growth factor- $\beta$ 1
<b>TNF-<math>\alpha</math></b>	Tumor necrosis factor- $\alpha$
<b>VEGF</b>	Vascular endothelial growth factor

## Biography



**Kara Spiller** is an Assistant Professor in Drexel University's School of Biomedical Engineering, Science, and Health Systems. Dr. Spiller received Bachelor's and Master's Degrees in Biomedical Engineering from Drexel in 2007. As an NSF Graduate Research Fellow, she conducted her doctoral research in the design of semi-degradable hydrogels for the repair of articular cartilage in the Biomaterials and Drug Delivery Laboratory at Drexel and in the Shanghai Key Tissue Engineering Laboratory of Shanghai Jiao Tong University. After completing her Ph.D. in 2010, she conducted research in the design of scaffolds for bone tissue engineering on a Fulbright Fellowship in the Biomaterials, Biodegradables, and Biomimetics (the 3Bs) Research Group at the University of Minho in Guimaraes, Portugal. She then conducted postdoctoral studies towards the development of immunomodulatory biomaterials for bone regeneration in the Laboratory for Stem Cells and Tissue Engineering at Columbia University, before joining the Faculty of Drexel in 2013. Her research is funded by grants from the National Science Foundation and the NIH, as well as grants from private foundations and industry. Her research interests include the role of inflammation in regenerative medicine, the design of immunomodulatory biomaterials, and international engineering education.

## References

1. Abraham A, et al. Machine learning for neuroimaging with scikitlearn. *Front. Neuroinform.* 2014; 8:14. [PubMed: 24600388]
2. Anderson JM, Rodriguez A, Chang DT. Foreign body reaction to biomaterials. *Semin. Immunol.* 2008; 20:86–100. [PubMed: 18162407]

3. Arnold L, et al. Inflammatory monocytes recruited after skeletal muscle injury switch into antiinflammatory macrophages to support myogenesis. *J. Exp. Med.* 2007; 204:1057–1069. [PubMed: 17485518]
4. Ashcroft GS, et al. Tumor necrosis factor- $\alpha$  (TNF- $\alpha$ ) is a therapeutic target for impaired cutaneous wound healing. *Wound Repair Regen.* 2012; 20:38–49. [PubMed: 22151742]
5. Badylak SF, Valentin JE, Ravindra AK, McCabe GP, Stewart-Akers AN. Macrophage phenotype as a determinant of biologic scaffold remodeling. *Tissue Eng. A.* 2008; 14:1835–1842.
6. Baluk P, et al. TNF- $\alpha$  drives remodeling of blood vessels and lymphatics in sustained airway inflammation in mice. *J. Clin. Investig.* 2009; 119:2954–2964. [PubMed: 19759514]
7. Benoit M, Desnues B, Mege J-L. Macrophage polarization in bacterial infections. *J. Immunol.* 2008; 181:3733. [PubMed: 18768823]
8. Berger ML, Mamdani M, Atkins D, Johnson ML. Good research practices for comparative effectiveness research: defining, reporting and interpreting nonrandomized studies of treatment effects using secondary data sources: the ISPOR Good Research Practices for Retrospective Database Analysis Task Force Report—Part I. *Value Health.* 2009; 12:1044–1052. [PubMed: 19793072]
9. Brown BN, Valentin JE, Stewart-Akers AM, McCabe GP, Badylak SF. Macrophage phenotype and remodeling outcomes in response to biologic scaffolds with and without a cellular component. *Biomaterials.* 2009; 30:1482–1491. [PubMed: 19121538]
10. Cooke M, et al. Comparison of cryopreserved amniotic membrane and umbilical cord tissue with dehydrated amniotic membrane/chorion tissue. *J. Wound Care.* 2014; 23:465–476. [PubMed: 25296347]
11. Davis JS, et al. The use of skin grafts in the ambulatory treatment of ulcers: report of fifty cases. *JAMA LXIV.* :558–560. 1915.
12. Duan-Arnold Y, et al. Retention of endogenous viable cells enhances the anti-inflammatory activity of cryopreserved amnion. *Adv. Wound Care (New Rochelle).* 2015; 4:523–533. [PubMed: 26401419]
13. Ferraro NM, Dampier W, Weingarten MS, Spiller KL. Deconvolution of heterogeneous wound tissue samples into relative macrophage phenotype composition via models based on gene expression. *Integr. Biol. (Camb.).* 2017; 9:328–338. [PubMed: 28290581]
14. Gibbons GW. Grafix, a cryopreserved placental membrane, for the treatment of chronic/stalled wounds. *Adv. Wound Care (New Rochelle).* 2015; 4:534–544. [PubMed: 26339532]
15. Guo X, et al. Modulation of cell attachment, proliferation, and angiogenesis by decellularized, dehydrated human amniotic membrane in in vitro models. *Wounds.* 2017; 29:28–38. [PubMed: 27852013]
16. Hao Y, Ma DH, Hwang DG, Kim WS, Zhang F. Identification of antiangiogenic and antiinflammatory proteins in human amniotic membrane. *Cornea.* 2000; 19:348–352. [PubMed: 10832697]
17. Hopkinson A, et al. Optimization of amniotic membrane (AM) denuding for tissue engineering. *Tissue Eng. C.* 2008; 14:371–381.
18. Huang G, et al. Accelerated expansion of epidermal keratinocyte and improved dermal reconstruction achieved by engineered amniotic membrane. *Cell Transplant.* 2013; 22:1831–1844. [PubMed: 23067579]
19. Jansky L, Reymanova P, Kopecky J. Dynamics of cytokine production in human peripheral blood mononuclear cells stimulated by LPS or infected by *Borrelia*. *Physiol. Res.* 2003; 52:593–598.
20. Johnson EL, Marshall JT, Michael GM. A comparative outcomes analysis evaluating clinical effectiveness in two different human placental membrane products for wound management. *Wound Repair Regen.* 2017; doi: 10.1111/wrr.12503
21. Laurent R, Nallet A, Obert L, Nicod L, Gindraux F. Storage and qualification of viable intact human amniotic graft and technology transfer to a tissue bank. *Cell Tissue Bank.* 2014; 15:267–275. [PubMed: 24633398]
22. Lavery LA, et al. The efficacy and safety of Grafix((R)) for the treatment of chronic diabetic foot ulcers: results of a multicentre, controlled, randomised, blinded, clinical trial. *Int. Wound J.* 2014; 11:554–560. [PubMed: 25048468]

23. Lavin Y, et al. Tissue-resident macrophage enhancer landscapes are shaped by the local microenvironment. *Cell*. 2014; 159:1312–1326. [PubMed: 25480296]
24. Law CW, Chen Y, Shi W, Smyth GK. Voom: precision weights unlock linear model analysis tools for RNA-seq read counts. *Genome Biol*. 2014; 15:R29. [PubMed: 24485249]
25. Leibovich SJ, Ross R. The role of the macrophage in wound repair. A study with hydrocortisone and anti-macrophage serum. *Am. J. Pathol*. 1975; 78:71–100. [PubMed: 1109560]
26. Litwiniuk M, Grzela T. Amniotic membrane: new concepts for an old dressing. *Wound Repair Regen*. 2014; 22:451–456. [PubMed: 25041617]
27. Liu D, Xiong H, Ning P, Chen J, Lan W. 2010 3rd International Conference on Biomedical Engineering and Informatics. 2010; 4:1633–1635.
28. Lurier EB, et al. Transcriptome analysis of IL-10-stimulated (M2c) macrophages by next-generation sequencing. *Immunobiology*. 2017; 222(7):847–856. [PubMed: 28318799]
29. Magatti M, et al. Human amnion favours tissue repair by inducing the M1-to-M2 switch and enhancing M2 macrophage features. *J. Tissue Eng. Regen. Med*. 2016; doi: 10.1002/term.2193
30. Markova A, Mostow EN. US skin disease assessment: ulcer and wound care. *Dermatol. Clin*. 2012; 30:107–111. [PubMed: 22117872]
31. Mirza R, DiPietro LA, Koh TJ. Selective and specific macrophage ablation is detrimental to wound healing in mice. *Am. J. Pathol*. 2009; 175:2454–2462. [PubMed: 19850888]
32. Mirza RE, Fang MM, Ennis WJ, Koh TJ. Blocking interleukin-1 $\beta$  induces a healing-associated wound macrophage phenotype and improves healing in Type 2 diabetes. *Diabetes*. 2013; 62:2579–2587. [PubMed: 23493576]
33. Mirza RE, Fang MM, Weinheimer-Haus EM, Ennis WJ, Koh TJ. Sustained inflammasome activity in macrophages impairs wound healing in Type 2 diabetic humans and mice. *Diabetes*. 2014; 63:1103–1114. [PubMed: 24194505]
34. Mirza R, Koh TJ. Dysregulation of monocyte/macrophage phenotype in wounds of diabetic mice. *Cytokine*. 2011; 56:256–264. [PubMed: 21803601]
35. Mosser DM, Edwards JP. Exploring the full spectrum of macrophage activation. *Nat. Rev. Immunol*. 2008; 8:958–969. [PubMed: 19029990]
36. Nassiri S, Zakeri I, Weingarten MS, Spiller KL. Relative expression of proinflammatory and antiinflammatory genes reveals differences between healing and nonhealing human chronic diabetic foot ulcers. *J. Investig. Dermatol*. 2015; 135:1700–1703. [PubMed: 25647438]
37. Niknejad H, Paeni-Vayghan G, Tehrani FA, Khayat-Khoei M, Peirovi H. Side dependent effects of the human amnion on angiogenesis. *Placenta*. 2013; 34:340–345. [PubMed: 23465536]
38. Parolini O, Caruso M. Review: preclinical studies on placenta-derived cells and amniotic membrane: an update. *Placenta*. 2011; 32(Suppl 2):S186–S195. [PubMed: 21251712]
39. Regulski M, et al. A retrospective analysis of a human cellular repair matrix for the treatment of chronic wounds. *Ostomy Wound Manag*. 2013; 59:38–43.
40. Roh JD, et al. Tissue-engineered vascular grafts transform into mature blood vessels via an inflammation-mediated process of vascular remodeling. *Proc. Natl Acad. Sci. USA*. 2010; 107:4669–4674. [PubMed: 20207947]
41. Sainson RCA, et al. TNF primes endothelial cells for angiogenic sprouting by inducing a tip cell phenotype. *Blood*. 2008; 111:4997–5007. [PubMed: 18337563]
42. Seabold, S., Josef, P. Statsmodels: econometric and statistical modeling with Python; Proceedings of the 9th Python in Science Conference; 2010. p. 57-61.
43. Sen CK, et al. Human skin wounds: a major and snowballing threat to public health and the economy. *Wound Repair Regen. Off. Publ. Wound Heal. Soc. Eur. Tissue Repair Soc*. 2009; 17:763–771.
44. Sindrilaru A, et al. An unrestrained proinflammatory M1 macrophage population induced by iron impairs wound healing in humans and mice. *J. Clin. Investig*. 2011; 121:985–997. [PubMed: 21317534]
45. Singh S, et al. Unbiased analysis of the impact of micropatterned biomaterials on macrophage behavior provides insights beyond predefined polarization states. *ACS Biomater. Sci. Eng*. 2017; doi: 10.1021/acsbomaterials.7b00104

46. Spiller KL, Koh TJ. Macrophage-based therapeutic strategies in regenerative medicine. *Adv. Drug Deliv. Rev.* 2017; doi: 10.1016/j.addr.2017.05.010
47. Spiller KL, et al. The role of macrophage phenotype in vascularization of tissue engineering scaffolds. *Biomaterials.* 2014; 35:4477–4488. [PubMed: 24589361]
48. Talmi YP, Sigler L, Inge E, Finkelstein Y, Zohar Y. Antibacterial properties of human amniotic membranes. *Placenta.* 1991; 12:285–288. [PubMed: 1754577]
49. Tseng SC, Li DQ, Ma X. Suppression of transforming growth factor-beta isoforms, TGF-beta receptor type II, and myofibroblast differentiation in cultured human corneal and limbal fibroblasts by amniotic membrane matrix. *J. Cell. Physiol.* 1999; 179:325–335. [PubMed: 10228951]
50. van Putten SM, Ploeger DTA, Popa ER, Bank RA. Macrophage phenotypes in the collagen-induced foreign body reaction in rats. *Acta Biomater.* 2013; 9:6502–6510. [PubMed: 23376130]
51. Wetzler C, Kamper H, Stallmeyer B, Pfeilschifter J, Frank S. Large and sustained induction of chemokines during impaired wound healing in the genetically diabetic mouse: prolonged persistence of neutrophils and macrophages during the late phase of repair. *J. Investig. Dermatol.* 2000; 115:245–253. [PubMed: 10951242]
52. Willenborg S, et al. CCR2 recruits an inflammatory macrophage subpopulation critical for angiogenesis in tissue repair. *Blood.* 2012; 120:613–625. [PubMed: 22577176]
53. Wilshaw SP, Kearney JN, Fisher J, Ingham E. Production of an acellular amniotic membrane matrix for use in tissue engineering. *Tissue Eng.* 2006; 12:2117–2129. [PubMed: 16968153]
54. Wilshaw SP, Kearney J, Fisher J, Ingham E. Biocompatibility and potential of acellular human amniotic membrane to support the attachment and proliferation of allogeneic cells. *Tissue Eng. A.* 2008; 14:463–472.
55. Witherel CE, Graney PL, Freytes DO, Weingarten MS, Spiller KL. Response of human macrophages to wound matrices in vitro. *Wound Repair Regen.* 2016; 24:514–524. [PubMed: 26874797]
56. Wolbank S, et al. Impact of human amniotic membrane preparation on release of angiogenic factors. *J. Tissue Eng. Regen. Med.* 2009; 3:651–654. [PubMed: 19701933]
57. Wynn TA, Barron L. Macrophages: master regulators of inflammation and fibrosis. *Semin. Liver Dis.* 2010; 30:245–257. [PubMed: 20665377]
58. Xue J, et al. Transcriptome-based network analysis reveals a spectrum model of human macrophage activation. *Immunity.* 2014; 40:274–288. [PubMed: 24530056]
59. Zheng Y, et al. Topical administration of cryopreserved living micronized amnion accelerates wound healing in diabetic mice by modulating local microenvironment. *Biomaterials.* 2017; 113:56–67. [PubMed: 27810642]





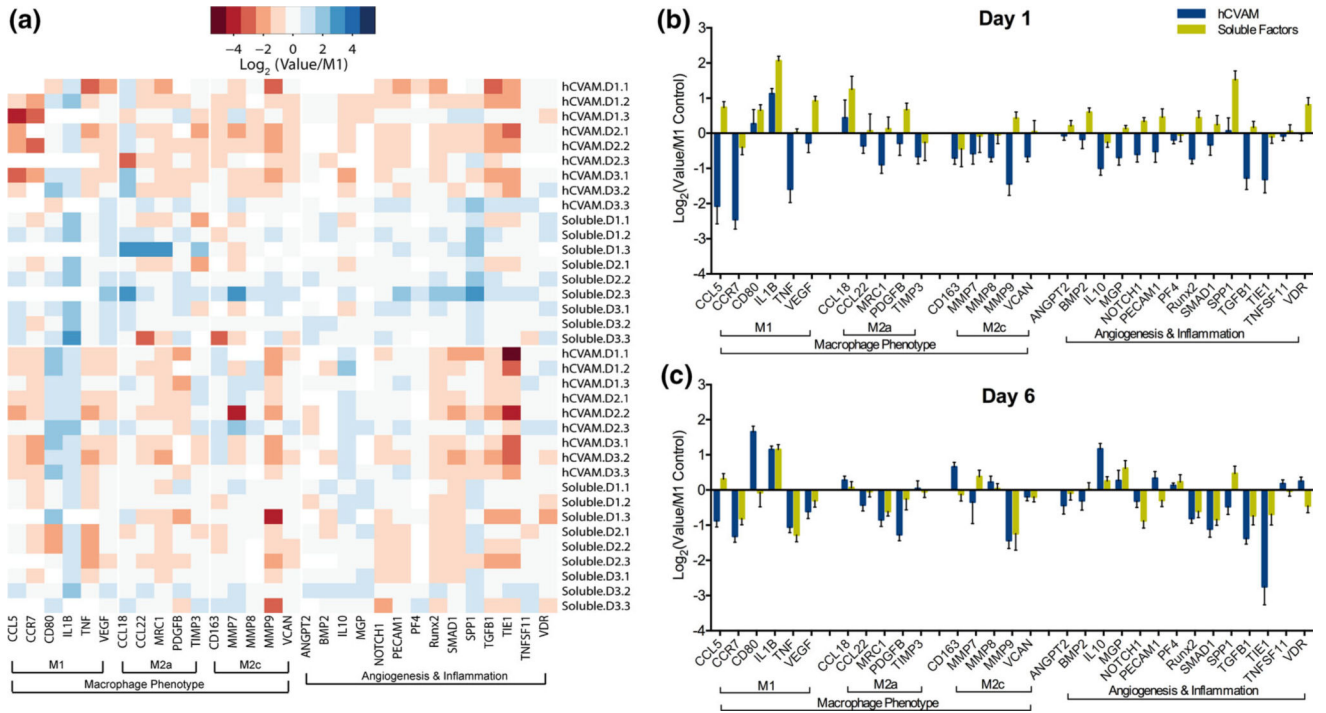


**FIGURE 2.**

(a) Heatmap of all gene replicates represented as  $\text{Log}_2(\text{value}/\text{M1 Control})$  generated in R using *heatmap.2* function in *gplots* package; (b) all genes and samples from NanoString gene expression analysis represented as a grouped column graph of  $\text{Log}_2(\text{Value}/\text{M1 Control})$  for day 1 and (c) day 6. A dotted line at a fold change of 1.0 (or 0 on graphs of  $\text{Log}_2$ -transformed data of values normalized to the M1 Control) represents no change vs. the M1 Control.

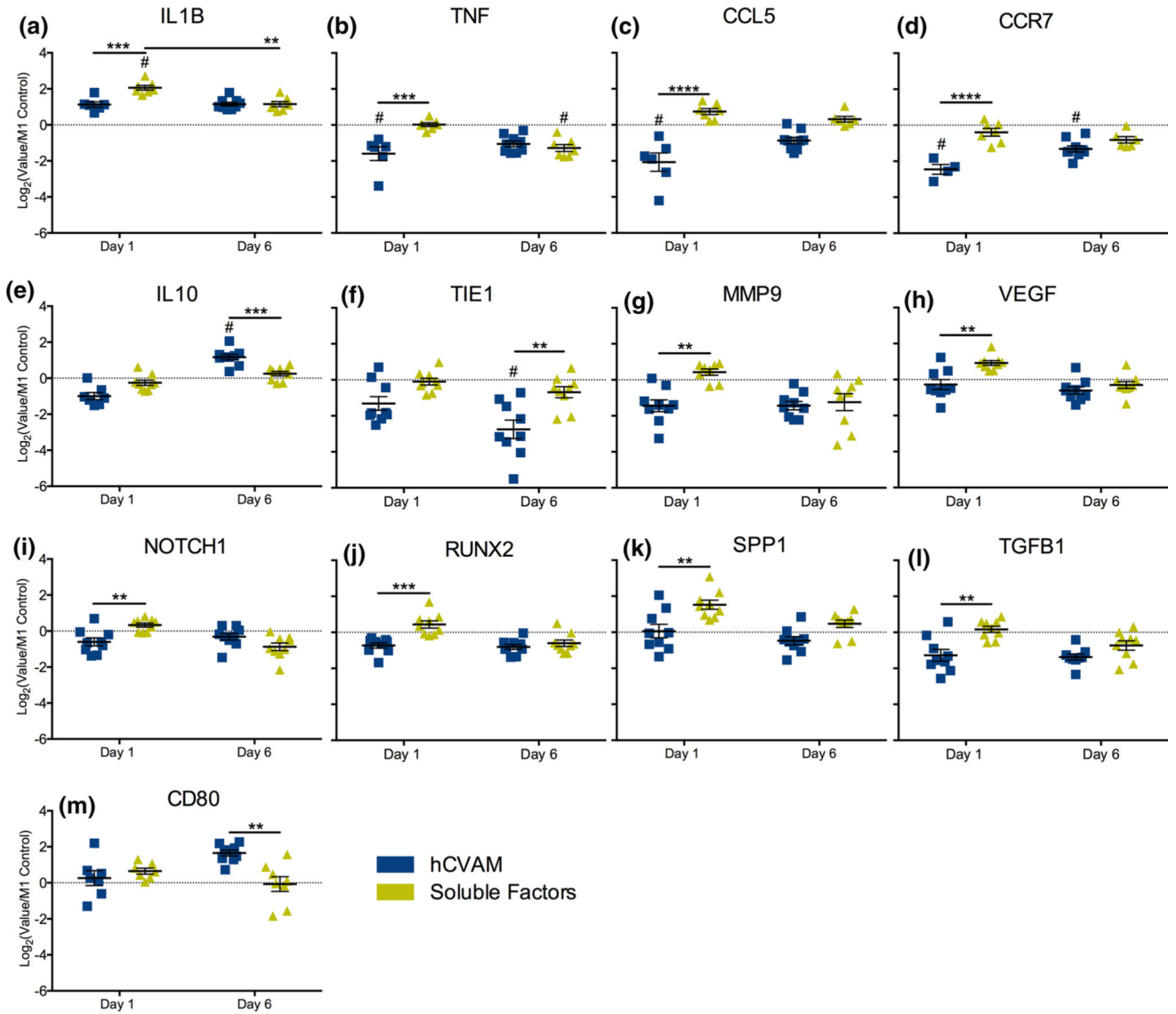


**FIGURE 3.**

NanoString gene expression analysis of all differentially expressed genes ( $p < 0.01$ ). hCVAM data are represented as  $\text{Log}_2(\text{Value}/\text{M1 Control})$  and as the mean of all experimental replicates ( $n = 4-9$ )  $\pm$  standard error of the mean (*SEM*). A dotted line at a fold change of 1.0 (or 0 on graphs of  $\text{Log}_2$ -transformed data of values normalized to the M1 Control) on each individual gene represents no change vs. the M1 Control; those samples significantly different from the M1 Control are shown with a # symbol ( $p < 0.01$ ). Statistical significance between treatment groups (represented with black bars) was calculated using a two-way ANOVA with a Tukey's post hoc multiple comparisons test, \* $p < 0.01$ , \*\* $p < 0.001$ , \*\*\* $p < 0.0001$ .

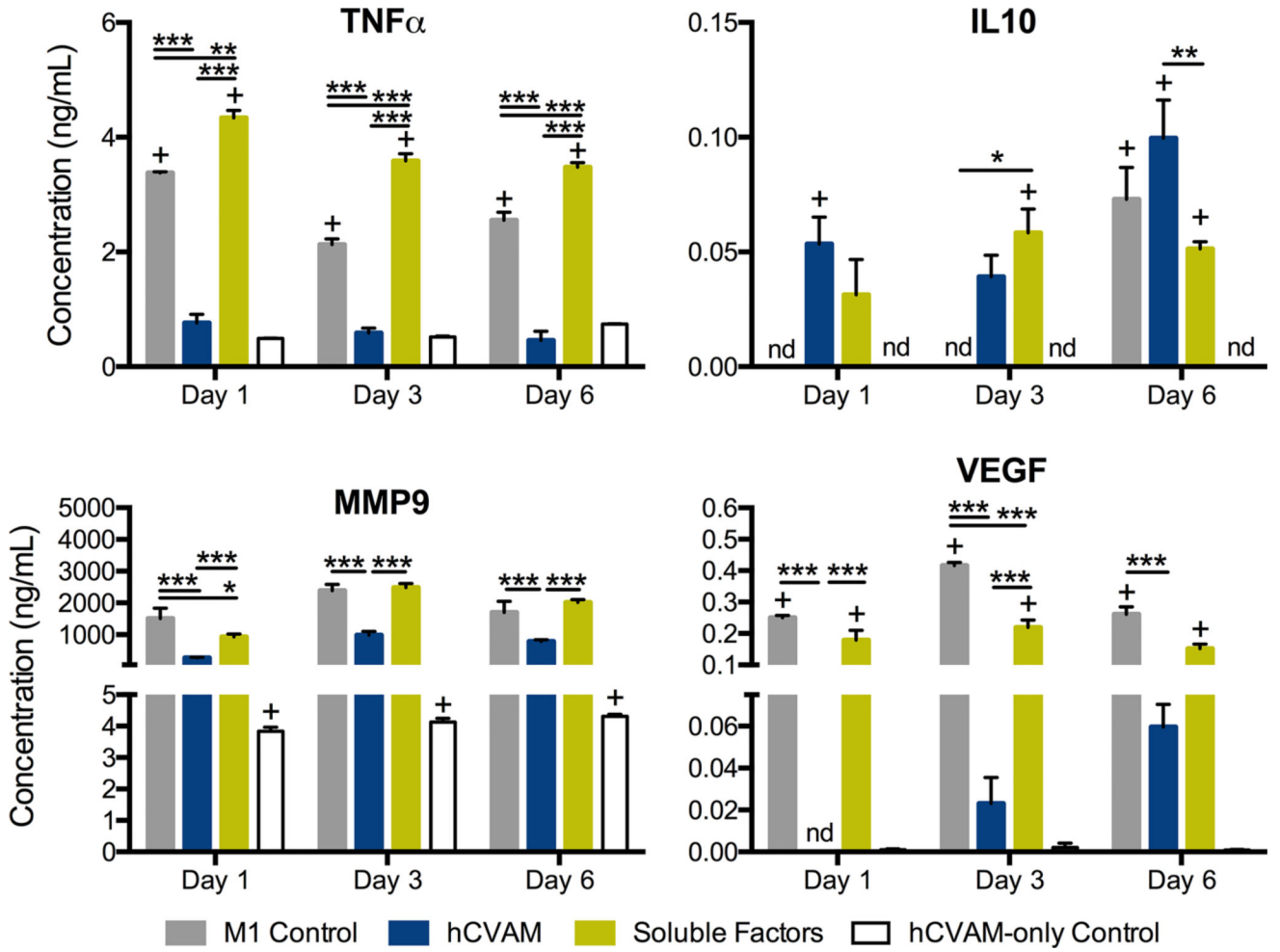


**FIGURE 4.** Protein content in the conditioned media generated from each treatment at days 1, 3, and 6. All data are represented as mean  $\pm$  SEM of all experimental replicates within detection limits ( $n = 3-9$  per treatment group per timepoint). Statistical analysis was performed using a two-way ANOVA with a Tukey's *post hoc* multiple comparisons analysis to determine differences between treatments within a time point, \* $p < 0.01$ , \*\* $p < 0.001$ , \*\*\* $p < 0.0001$ , + $p < 0.01$  compared to the hCVAM Control, and nd = no detection of protein.

TABLE 1

NanoString custom codeset.

Code classes	Names	Accession #
Endogenous	ALPL	NM_000478.4
Endogenous	ANGPT1	NM_001146.3
Endogenous	ANGPT2	NM_001147.2
Endogenous	BGLAP	NM_199173.3
Endogenous	BMP2	NM_001200.2
Endogenous	CCL18	NM_002988.2
Endogenous	CCL22	NM_002990.3
Endogenous	CCL5	NM_002985.2
Endogenous	CCR7	NM_001838.2
Endogenous	CD163	NM_004244.4
Endogenous	CD80	NM_005191.3
Endogenous	COL1A1	NM_000088.3
Endogenous	COL4A1	NM_001845.4
Endogenous	CTGF	NM_001901.2
Endogenous	IL10	NM_000572.2
Endogenous	IL1B	NM_000576.2
Endogenous	MGP	NM_000900.2
Endogenous	MMP7	NM_002423.3
Endogenous	MMP8	NM_002424.2
Endogenous	MMP9	NM_004994.2
Endogenous	MRC1	NM_002438.2
Endogenous	NOTCH1	NM_017617.3
Endogenous	PDGFB	NM_033016.2
Endogenous	PECAM1	NM_000442.3
Endogenous	PF4	NM_002619.2
Endogenous	Runx2	NM_004348.3
Endogenous	SMAD1	NM_005900.2
Endogenous	SPP1	NM_000582.2
Endogenous	TEK	NM_000459.3
Endogenous	TGFB1	NM_000660.3
Endogenous	TIE1	NM_005424.2
Endogenous	TIMP3	NM_000362.4
Endogenous	TNF	NM_000594.2
Endogenous	TNFSF11	NM_003701.2
Endogenous	VCAN	NM_004385.3
Endogenous	VDR	NM_000376.2
Endogenous	VEGF	NM_001025366.1
Housekeeping	GAPDH	NM_002046.3
Housekeeping	GUSB	NM_000181.1

Code classes	Names	Accession #
Housekeeping	HMBS	NM_000190.3
Housekeeping	RPS9	NM_001013.3
Housekeeping	SDHA	NM_004168.2
Negative	NEG_A	ERCC_00096.1
Negative	NEG_B	ERCC_00041.1
Negative	NEG_C	ERCC_00019.1
Negative	NEG_D	ERCC_00076.1
Negative	NEG_E	ERCC_00098.1
Negative	NEG_F	ERCC_00126.1
Negative	NEG_G	ERCC_00144.1
Negative	NEG_H	ERCC_00154.1
Positive	POS_A	ERCC_00117.1
Positive	POS_B	ERCC_00112.1
Positive	POS_C	ERCC_00002.1
Positive	POS_D	ERCC_00092.1
Positive	POS_E	ERCC_00035.1
Positive	POS_F	ERCC_00034.1

Author Manuscript

Author Manuscript

Author Manuscript

Author Manuscript